Rechargeable Li/Cl_2 battery down to -80 °C

*Peng Liang, Guanzhou Zhu, Cheng-Liang Huang, Yuan-Yao Li, Hao Sun, Bin Yuan, Shu-Chi Wu, Jiachen Li, Feifei Wang, Bing-Joe Hwang, and Hongjie Dai**

P. Liang, G. Zhu, S.-C. Wu, J. Li, H. Dai
Department of Chemistry and Bio-X, Stanford University, Stanford, CA 94305, USA
E-mail: hdai1@stanford.edu
Peng Liang and Guanzhou Zhu contributed equally to this work.

C.-L. Huang, Y.-Y. Li
Department of Chemical Engineering, National Chung Cheng University, Chia-Yi, 62102, Taiwan

C.-L. Huang
Department of Electrical Engineering, National Chung Cheng University, Chia-Yi, 62102, Taiwan

H. Sun, B. Yuan
Frontiers Science Center for Transformative Molecules, School of Chemistry and Chemical Engineering, and Zhangjiang Institute for Advanced Study, Shanghai Jiao Tong University, Shanghai, 200240, China

F. Wang
Department of Electrical and Electronic Engineering, The University of Hong Kong, Hong Kong, 999077, Hong Kong

B.-J. Hwang
Department of Chemical Engineering, National Taiwan University of Science and Technology, Taipei, 106, Taiwan

Keywords: rechargeable lithium/chlorine battery, ultra-low temperature, high-capacity, Cl_2 trapping, thionyl chloride ($SOCl_2$)

Low temperature rechargeable batteries are important to life in cold climates, polar/deep-sea expeditions and space explorations. Here, we report 3.5 - 4 V rechargeable lithium/chlorine (Li/Cl_2) batteries operating down to -80 °C, employing Li metal negative electrode, a novel CO_2 activated porous carbon (KJCO_2) as the positive electrode, and a high ionic conductivity (~ 5 to 20 mS cm^{-1} from -80 °C to room-temperature) electrolyte comprised of aluminum chloride ($AlCl_3$), lithium chloride (LiCl), and lithium bis(fluorosulfonyl)imide (LiFSI) in low-

melting-point (-104.5 °C) thionyl chloride ($SOCl_2$). Between room-temperature and -80 °C, the Li/Cl_2 battery delivered up to ~ 29,100 - 4,500 mAh g^{-1} first discharge capacity (based on carbon mass) and a 1,200 - 5,000 mAh g^{-1} reversible capacity over up to 130 charge-discharge cycles. Mass spectrometry and X-ray photoelectron spectroscopy probed Cl_2 trapped in the porous carbon upon LiCl electro-oxidation during charging. At -80 °C, Cl_2/SCl_2/S_2Cl_2 generated by electro-oxidation in the charging step were trapped in porous $KJCO_2$ carbon, allowing for reversible reduction to afford a high discharge voltage plateau near ~ 4 V with up to ~ 1000 mAh g^{-1} capacity for SCl_2/S_2Cl_2 reduction and up to ~ 4000 mAh g^{-1} capacity at ~ 3.1 V plateau for Cl_2 reduction.

1. Introduction

Existing rechargeable batteries underperform at low temperatures (< ~ -30 °C) with reduction in battery capacity and cycle-life, limiting the operation of electronic devices, electric vehicles and equipment in polar climates, subsea and space explorations.[1-6] Li-ion batteries with ethylene carbonate (EC)-based electrolytes can function down to ~ -20 °C,[7] limited by decreased ionic conductivity, slower interfacial charge transfer kinetics and Li^+ transport in electrodes.[8-14] Developing new rechargeable batteries at low temperatures down to -80 °C has been challenging,[15-19] especially for batteries with high specific capacity and energy density.

The lithium-thionyl chloride (Li-$SOCl_2$) primary batteries are well known for their high energy density and wide use in professional electronics and industrial instruments, but lacks rechargeability.[20, 21] Although at room temperature (RT), we converted Li-$SOCl_2$ primary batteries into Na/Cl_2 (or Li/Cl_2) secondary batteries via mainly redox between Cl_2/Cl^- at the positive electrode and Na/Na^+ (or Li/Li^+) redox at the negative electrode, [20, 21] thus far rechargeable Li/Cl_2 batteries remains unexplored below room temperature (RT) due to the limitation of electrolyte and positive electrode material. More importantly, the Li/Cl_2 battery chemistry at low temperature is largely unknow.[22-25]

Here, we investigate an ultra-low temperature Li/Cl_2 battery using a Li metal as the negative electrode, Ketjenblack (KJ) carbon black activated in carbon dioxide (CO_2) at 1000 °C for 45 min ($KJCO_2$, see Methods) as the positive electrode, and $AlCl_3$/LiCl/LiFSI/dissolved in $SOCl_2$ as the electrolyte. The newly engineered electrolyte affords high Li^+ transference number (t_{Li+} = 0.951) at RT, low viscosity and high ionic conductivity at low temperatures (5.26 mS cm^{-1} at -80 °C) using 1.0 M $AlCl_3$, and stable passivation of the Li metal anode with a solid-electrolyte-interface (SEI) rich in LiCl/LiF. Also important is high temperature CO_2 activation of KJ carbon affording ~ 2X increase in surface area (~ 2386.9 m^2 g^{-1}) and pore volume (~ 6.5

cm^3 g^{-1}) for the positive electrode and giving much more LiCl deposition during the first discharge for subsequent reversible LiCl/Cl_2 redox reactions, and delivering up to ~ 30,000 mAh g^{-1} first discharge capacity (~3.55 V), which is the highest capacity known to date. The resulting batteries deliver a 1,200 - 5,000 mAh g^{-1} reversible capacity operating between room-temperature (25 °C) and -80 °C. By X-ray and mass spectroscopy, we studied the battery reaction chemistry and analyzed the main reactive species generated by battery charging at -40 °C to -80 °C and trapped in porous carbon including SCl_2/S_2Cl_2, $SOCl_2$, SO_2Cl_2 and Cl_2, shedding light to battery rechargeability at low temperatures.

2. Results and Discussion

2.1. The first discharge of Li/KJCO$_2$ batteries

We constructed CR2032 coin cell (20 mm diameter x 3.2 mm thickness) batteries by using a Li metal as the negative electrode, either KJ (Li/KJ battery) or KJCO$_2$ (Li/KJCO$_2$ battery) as the positive electrode in an electrolyte comprised of 1.0 M $AlCl_3$ + 0.95 M LiCl dissolved in $SOCl_2$ with 0.05 M of LiFSI additive (**Figure 1**a, see Methods). The as received KJ material (EC-600JD, Figure 1b) showed signs of etching and apparent reduction in size after activation in CO_2 at 1000 ºC for 45 minutes (Figure 1c), accompanied by a mass loss of ~ 85% due to the reaction CO_2 (g) + C (s) →2 CO (g).[20, 21] Raman spectroscopy showed increased defects and disorder (Figure S1a),[26] with a complete disappearance of graphitic ordering in X-ray diffraction after the CO_2 activation step (Figure S1b).[27]

At RT, the Li/KJCO$_2$ battery showed a 2X higher first discharge capacity than Li/KJ cell (~ 15,300 mAh g^{-1} or 30.6 mAh cm^{-2} and ~ 29,100 mAh g^{-1} or 58.2 mAh cm^{-2} for KJ and KJCO$_2$ respectively; current = 50 mA g^{-1}, Figure 1d) with a ~ 3.55 V discharge voltage. Note that throughout this work, specific capacity and areal specific capacity were based on mass of loaded carbon in the positive electrode (~ 2 mg cm^{-2}) and electrode area (~ 1.767 cm^2) respectively, as commonly done for Li/air or Li/O_2 batteries.[28] Higher KJCO$_2$ mass loading of ~ 6 mg cm^{-2} still afforded an impressive first discharge capacity of ~ 9,407 mAh g^{-1} at the same current (Figure S2). The first discharge (~ 3.55 V plateau) was due to Li metal oxidation to Li^+ on the negative electrode and the $SOCl_2$ reduction to sulfur (S), sulfur dioxide (SO_2) and LiCl deposited on the porous carbon positive electrode (2 $SOCl_2$ + 4 Li^+ + 4 e^- → S + SO_2 + 4 LiCl), accompanied by a discernible ~ 3.2 V plateau attributed to reduction of SO_2.[20, 21, 29, 30] The CO_2 activation process doubled the specific surface area (from 1307.4 m^2 g^{-1} to 2386.9 m^2 g^{-1}) and pore volume for KJ to KJCO$_2$ (from 3.1 cm^3 g^{-1} to 6.5 cm^3 g^{-1}) (Figure 1e and Table S1), allowing for increased deposition of LiCl and higher discharge capacity (Figure 1d).[20, 31] High

surface area and large pore volume of carbon materials are also found important to the reversible specific capacity of secondary Na/Cl_2 batteries.[20]

At low temperatures, the Li/$KJCO_2$ battery delivered first discharge voltage/capacity of 3.4 V/8,521 mAh g^{-1}, 3.3 V/5,532 mAh g^{-1}, and 3.1 V/4,503 mAh g^{-1} at -20 ℃, -40 ℃ and -80 ℃, respectively (**Figure 2**a). LiCl deposition on $KJCO_2$ was confirmed by XRD (Figure 2b), both in the pores of $KJCO_2$ and on the surfaces of $KJCO_2$ until passivation (see schematic in Figure 2c).[20, 21] This was consistent with that pore volumes of carbon materials in the positive electrode positively correlated with the first discharge capacity of primary batteries and in recent secondary batteries.[20, 21, 31-34] Based on the $SOCl_2$ reduction reaction equation and the first discharge capacity, the estimated deposited LiCl volume was ~ 0.07 cm^3, ~ 0.027 cm^3, ~ 0.013 cm^3 and ~ 0.011 cm^3 at RT, -20 °C, -40 °C and -80 °C respectively compared to the total pore volume ~ 0.023 cm^3 in the $KJCO_2$ electrode.

LiCl deposition on $KJCO_2$ decreased with reduced discharge capacity at lower temperatures (Figure 2a) due to increased electrolyte viscosity (Figure S3), decreased Li^+ and Cl^- ion diffusion,[22, 23, 35] and lower electrolyte conductivity from 20.34 mS cm^{-1} at room temperature to 5.26 mS cm^{-1} at -80 °C (Figure 2d). Due to slower growth kinetics of crystallites at lower temperatures,[22, 23, 35] the size of LiCl crystallites deposited on the electrode decreased from > 3 μm at room temperature (Figure 2e) to ~ 1.5 μm, ~ 200 nm and ~ 60 nm at -20 ℃, -40 ℃ and -80 ℃ respectively (Figure 2f-h) accompanied by weaker XRD patterns (Figure 2b).

The 1 M neutral electrolyte and low melting point (-104.5 °C) of $SOCl_2$ were important to battery operation down to -80 ℃ owing to low electrolyte viscosity than those in our previous alkali metal/Cl_2 batteries (with higher 4M or 1.8 M $AlCl_3$, Figure S4).[20-22] Through CO_2 activation of a common carbon black material and electrolyte tuning, we obtained a record setting first discharge capacity up to ~ 30,000 mAh g^{-1} with flat ~ 3.55 V discharge plateau, an important result on its own right in terms of high energy density Li/$SOCl_2$ primary batteries.

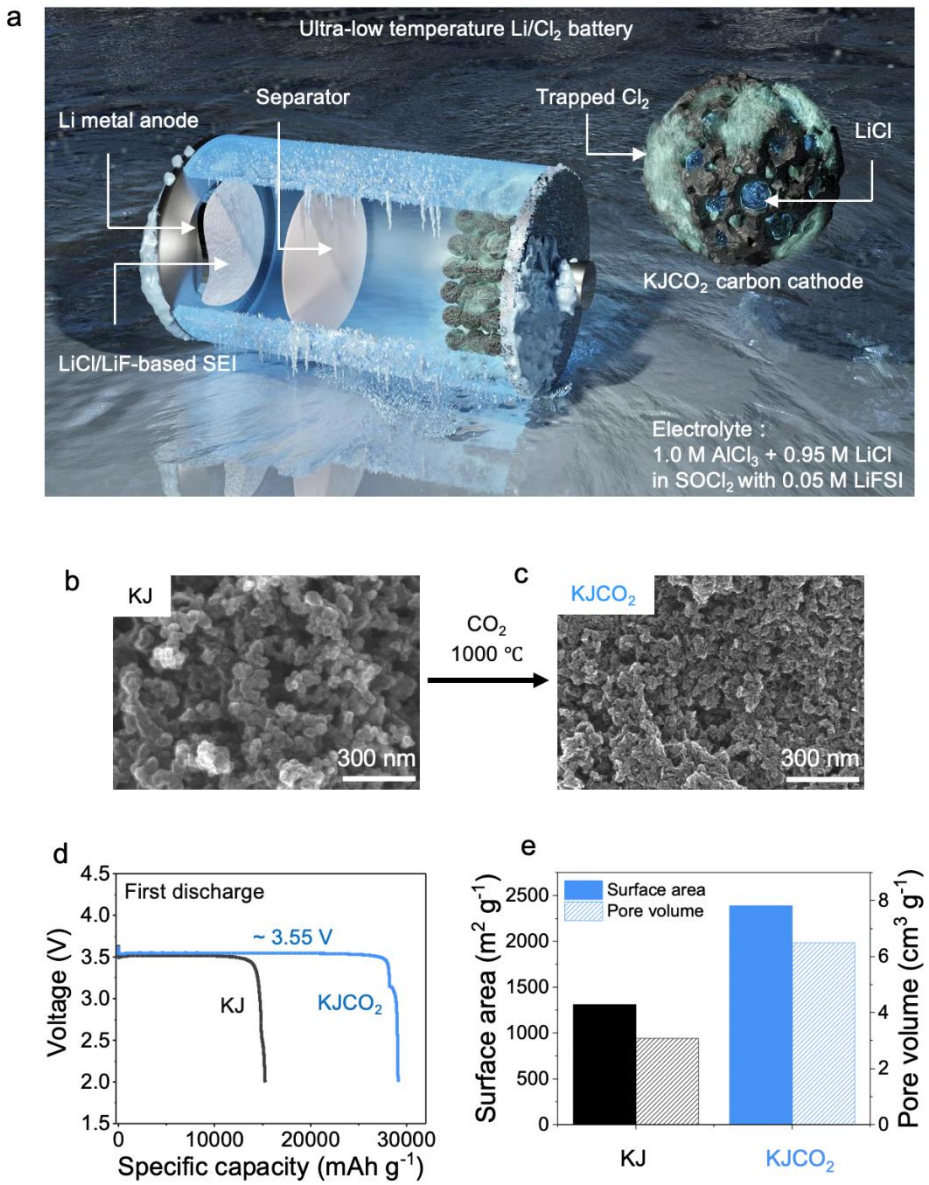

Figure 1. Ultrahigh first discharge capacity of a Li/porous-carbon battery at room temperature. a) Schematic drawing of an ultra-low temperature Li/Cl_2 battery. b, c) SEM images of pristine KJ (b) and high temperature activated $KJCO_2$ (c) at the same magnification. d) The first discharge curves of room temperature batteries using either KJ (black) or $KJCO_2$ (blue) recorded at 50 mA g^{-1}. Notice the drastic discharge capacity increase when $KJCO_2$ was the positive electrode. e) Average measured Brunauer–Emmett–Teller (BET) surface area, pore volume (micropores and mesopores) of pristine KJ (black) or $KJCO_2$ (blue). The loading of KJ or $KJCO_2$ was ~ 2.0 mg cm^{-2} in the positive electrodes for the Li/KJ or Li/$KJCO_2$ batteries.

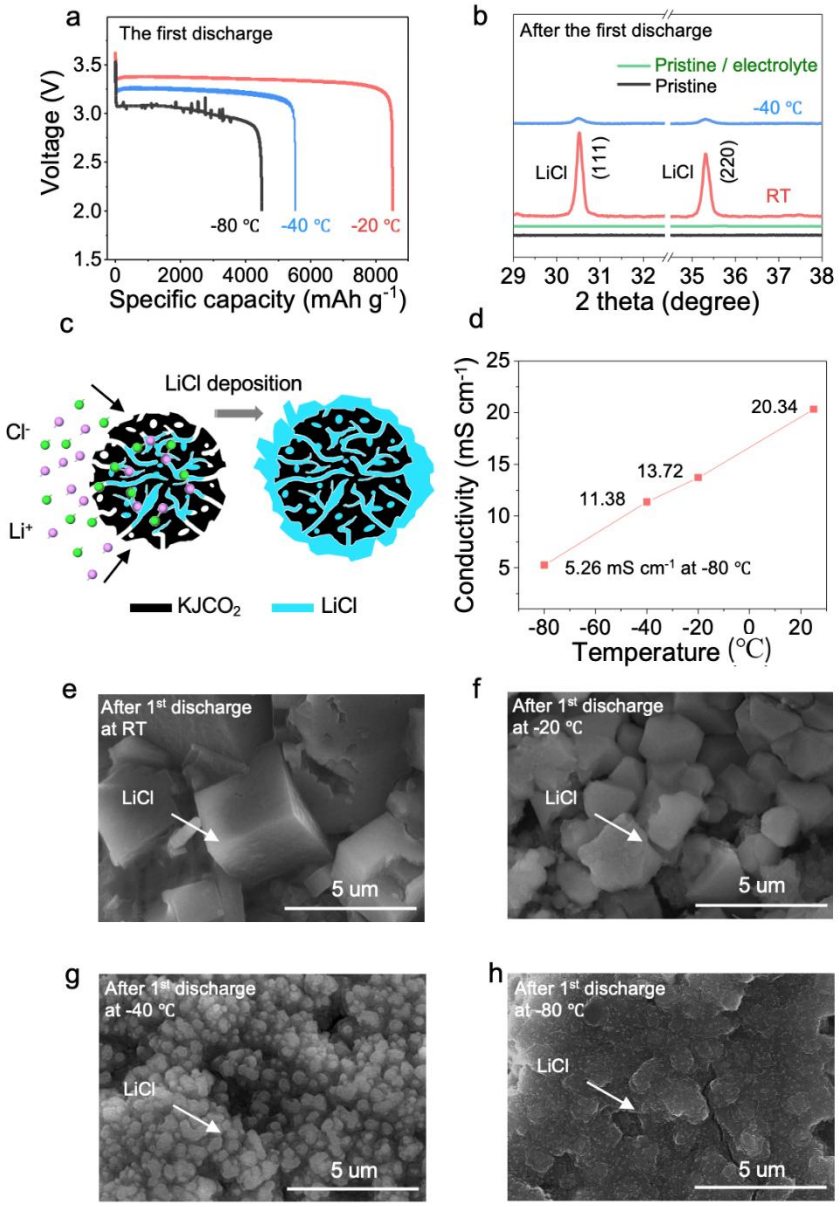

Figure 2. The first discharge characteristics of Li/$KJCO_2$ batteries at low temperatures. a) The first discharge curves of Li/$KJCO_2$ batteries at -20 ℃, -40 ℃ and -80 ℃ respectively. The current was 50 and 12.5 mA g^{-1} for -20/-40 ℃ and -80 ℃, respectively. b) XRD of pristine $KJCO_2$ electrode (black), pristine $KJCO_2$ electrode simply soaked in electrolyte and dried (green, used as a control sample), and $KJCO_2$ electrode after the battery's first discharge at room temperature (red) and -40 ℃ (blue). LiCl was formed on the $KJCO_2$ electrode after first discharge, indicated by the strong LiCl XRD peaks. c) Schematic drawing of the LiCl deposition in the pores and on the surface of $KJCO_2$. d) The measured ionic conductivity of the electrolyte (1.0 M $AlCl_3$ + 0.95 M LiCl dissolved in $SOCl_2$ with 0.05 M of LiFSI additive) at different temperatures. e-h) SEM images of $KJCO_2$ electrode after the first discharge at RT, -20 ℃, -40 ℃ and -80 ℃, showing different morphologies/reduced sizes of the deposited LiCl. The loading of $KJCO_2$ was ~ 2.0 mg cm^{-2} on the positive electrodes of all batteries.

2.2. Secondary batteries operating at low temperatures at -20 °C, -40 °C and -80 °C.

In the temperature range of RT to -20 °C, after the first discharge the Li/$KJCO_2$ cell was rechargeable and cyclable at 1200 mAh g^{-1} capacity (areal capacity ~ 2.4 mAh cm^{-2}, current 100 mA g^{-1}, C/12) with up to ~ 70 cycle-life (Figure S5a-d). Rechargeability mainly stemmed from reversible LiCl/Cl_2 redox reactions on the positive electrode, i.e., Cl_2 was generated by LiCl oxidation during charging and trapped in the pores of $KJCO_2$, and reduced to LiCl upon discharge.[20, 21] At RT, the first discharge plateau at 3.55 V (Figure 1d) was lower than the subsequent discharge (3.61 V, Figure S5b) due to $SOCl_2$ vs. Cl_2 reduction (also observed previously for Na/Cl_2 cells,[20] but the difference disappeared at low temperature due to higher polarization (Figure S5e) caused by increased electrolyte viscosity (Figure S3) and lower electrolyte conductivity (Figure 2d). Note that throughout this work, charging was controlled by setting the charging time at a specific capacity (= cycling capacity/current) and discharge proceeded down to a cut-off voltage of 2.0 V (see Methods).

At -40 °C, the Li/$KJCO_2$ battery exhibited improved cycle life over ~ 130 cycles with 1200 mAh g^{-1} (~ 2.4 mAh cm^{-2}) capacity under 100 mA g^{-1}/0.2 mA cm^{-2} current (C/12), with an average coulombic efficiency (CE) was ~ 100% (**Figure 3**a). Further, the battery showed cyclability at a higher specific capacity of 2500 mAh g^{-1} (areal capacity: ~ 5 mAh cm^{-2} per cycle) at -40 °C over > 75 cycles (Figure 3b), much improved over at -20 °C (< 15 cycles, Figure S6a, b). Continued increasing of the cycling capacities to 4000 mAh g^{-1} (areal capacity ~ 8 mAh cm^{-2}) and 5000 mAh g^{-1} (areal capacity ~ 10 mAh cm^{-2}) still exhibited rechargeability/cyclability albeit with a reduced cycle-life of < 10 cycles (Figure 3c, d). At higher rate, the -40 °C Li/$KJCO_2$ battery was able to perform charge and discharge (at the same rate) at 2500 mAh g^{-1} capacity and cycle stably at current up to 400 mA g^{-1} (C/6.25, ~ 0.8 mA cm^{-2}, Figure S6c) with a slight increase in charge-discharge polarization voltage/overpotential (Figure S6d).

The battery's CE initially deviated from 100% (Figure 3a-d), suggesting an "in situ activation" processes such as anionic intercalation/expanding/exfoliation of disordered carbon layers in the positive electrode as the battery started charging and cycling.[21] This allowed slightly more $SOCl_2$ to be reduced after each charging in the beginning cycles, giving an increasing CE to > 100%. Such 'in-situ activation' allowed the positive electrode to host additional LiCl and electrolyte, and improve the electrolyte wetting during its subsequent discharging step, especially at low temperature. After the initial few cycles, the 'in-situ activation' stopped, and the battery reached its stable cycling stage to reach ~ 100% CE. The decrease in capacity/Coulombic efficiency (< 100%) in the last few cycles might be due to a

worsening of the positive electrode's ability to host Cl_2, and the less reversible of redox reactions of $LiCl/Cl_2$ over cycling.[20, 21]

The high cycling capacity of our Li/$KJCO_2$ battery at -40 °C (1200 mAh g^{-1}, > 130 cycles; 2500 mAh g^{-1}, > 75 cycle) and ~ 3.3 V discharging plateau (Figure 3e) encouraged us to employ a Li/$KJCO_2$ CR2032 coin cell charged to 5000 mAh g^{-1} to power an electronic watch purchased from Amazon operating at a voltage of 3.0 V in a -40 °C freezer. The fully charged battery powered the watch at -40 °C over ~ 6 months (Figure 3f) on one charging.

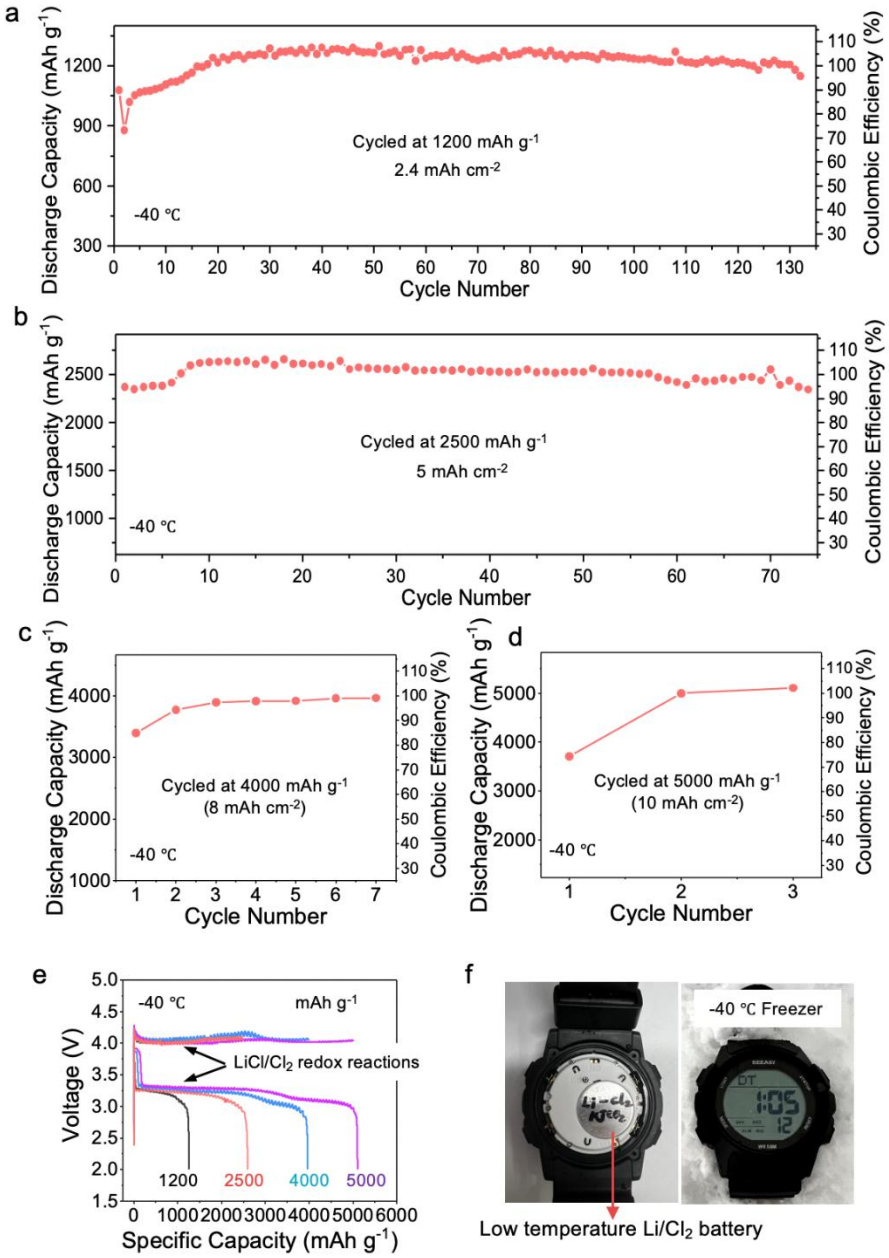

Figure 3. The cycling characteristics of Li/$KJCO_2$ batteries at -40 °C. a-d) Cycling performance of a Li/$KJCO_2$ battery at 1200 mAh g^{-1} (a), 2500 mAh g^{-1} (b), 4000 mAh g^{-1} (c), and 5000 mAh g^{-1} (d) cycling capacity under 100 mA g^{-1} current at -40 °C. e) Charge-discharge curves of Li/$KJCO_2$ batteries at 1200 - 5000 mAh g^{-1} cycling capacities under 100 mA g^{-1} current at -

40 ℃. f) Photos showing a commercial electronic watch powered by a fully charged Li/$KJCO_2$ battery coin cell (CR2032) in a -40 ℃ freezer over 6 months. The loading of $KJCO_2$ was ~ 2.0 mg cm^{-2} in all batteries in this figure.

At -80 °C, the Li/$KJCO_2$ batteries (placed in a biological freezer) cycled stably at 1200 mAh g^{-1} over ~ 70 cycles with near ~100 % average CE (**Figure 4**a, current 25 mA g^{-1}/0.05 mA cm^{-2}, C/48). At this rate batteries were also cyclable at higher specific capacity of 2500 mAh g^{-1} (Figure 4b), 4000 mAh g^{-1} (Figure 4c) and even ~ 5000 mAh g^{-1} (Figure S7), but with shorter cycle lives. At -80 °C, the main battery charging plateau of ~ 4.25 V and discharging plateau of ~3.1 V discharging plateau were attributed to oxidation of LiCl to Cl_2 and the reduction of Cl_2 back to LiCl, respectively (Figure 4d). In addition to LiCl oxidation on $KJCO_2$, charging to higher capacities also led to increased oxidation of $SOCl_2$ in the electrolyte to form SCl_2/S_2Cl_2, especially when charging to ~ 5000 mAh g^{-1} during which a pronounced increase in charging voltage was observed (Figure 4d). This was also consistent with the appearance of an impressive high discharge voltage plateau at ~ 3.8 V, with a specific capacity up to 1000 mAh g^{-1} (Figure 4d) due to reduction of the SCl_2/S_2Cl_2 generated in the charging step.[20, 21, 29] The discharge plateaus at ~ 3.1 V and ~ 2.9 V corresponded to reduction of Cl_2 and SO_2Cl_2, respectively (Figure 4d).[20, 21] Note that the C-rate (charging/discharging time) of our ultra-low temperature Li/Cl_2 battery is not outstanding due to the high rechargeable capacities (1200 to 5000 mAh g^{-1}), but our battery delivers competitive currents at -40 ℃ and -80 ℃ over other low temperature Li-ion batteries and are superior in cycle-life and areal capacity (see Table S2).

We employed a battery placed in a -80 °C freezer (Figure 4e-g) charged to ~ 5000 mAh g^{-1} to power a light-emitting diode (LED) (with operating voltage > 3.0 V; Figure 4f shows electrolyte remained as a liquid at -80 °C).

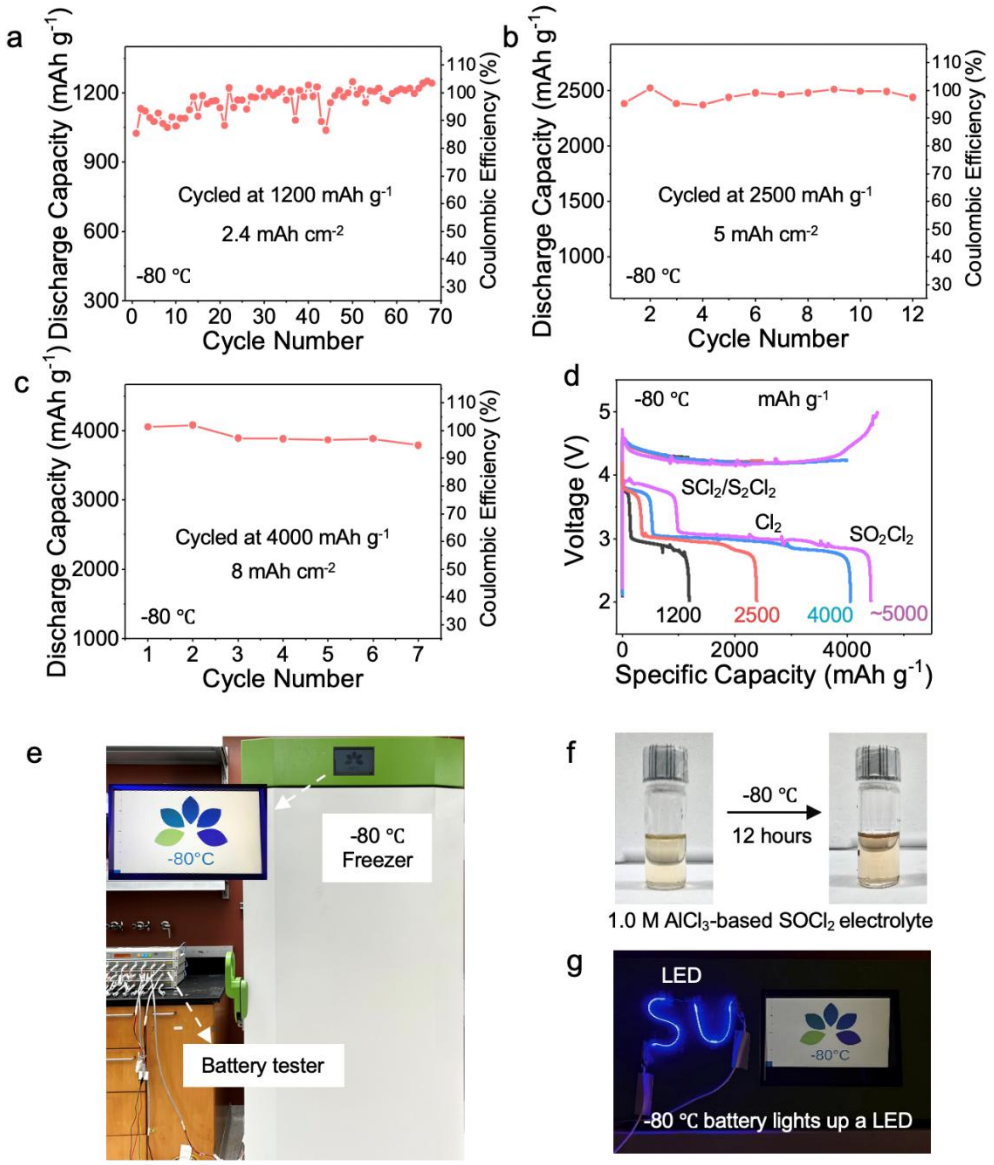

Figure 4. The cycling characteristics of Li/$KJCO_2$ batteries at ultra-low temperature (-80 ℃). a-c) Cycling performance of a Li/$KJCO_2$ battery with 1200 mAh g^{-1} (a), 2500 mAh g^{-1} (b), and 4000 mAh g^{-1} (c) cycling capacity under 25 mA g^{-1} current at -80 ℃. d) Charge-discharge curves of Li/$KJCO_2$ batteries with 1200 - ~ 5000 mAh g^{-1} cycling capacities under 25 mA g^{-1} current at -80 ℃ (Note that the voltage limit of battery tester was 5.0 V). e) The -80 ℃ freezer and battery testers used for low temperature battery electrochemical measurements. f) Photographs of 1.0 M $AlCl_3$-based $SOCl_2$ electrolyte used for low temperature Li/$KJCO_2$ battery after being frozen in a -80 ℃ freezer overnight. g) Lighting up an LED using a -80 ℃ Li/$KJCO_2$ battery coin cell (CR2032). The lighted LED outside the -80 ℃ freezer was connected by wires to the battery inside the -80 ℃ freezer. The loading of $KJCO_2$ was ~ 2.0 mg cm^{-2} in all batteries in this figure.

2.3. Spectroscopic investigation of battery reactions on the positive electrode side

For batteries after cycling at -40 °C, SEM imaging showed the formation of 200 - 300 nm LiCl on $KJCO_2$ (Figure S8a) corresponding to reduction of trapped Cl_2 to LiCl.[20, 21] Upon charging from 1200 to 5000 mAh g^{-1}, the deposited LiCl were increasingly removed/oxidized (SEM in Figure S8b, c and EDX mapping in Figure S8d) accompanied by decreases in the battery electrochemical impedance (Figure S9). The formation of Cl_2 (2 LiCl → 2 Li^+ + Cl_2 + 2 e^-) constituted the main charging capacity,[20, 21] and reduction of trapped Cl_2 in $KJCO_2$ constituted the main discharge plateau, giving the main charge/discharge 4.01 V/3.3 V plateaus (Figure 3e) with an overall battery reaction of Li + 1/2 Cl_2 ↔ LiCl at - 40 °C (see Schematic in **Figure 5**a).

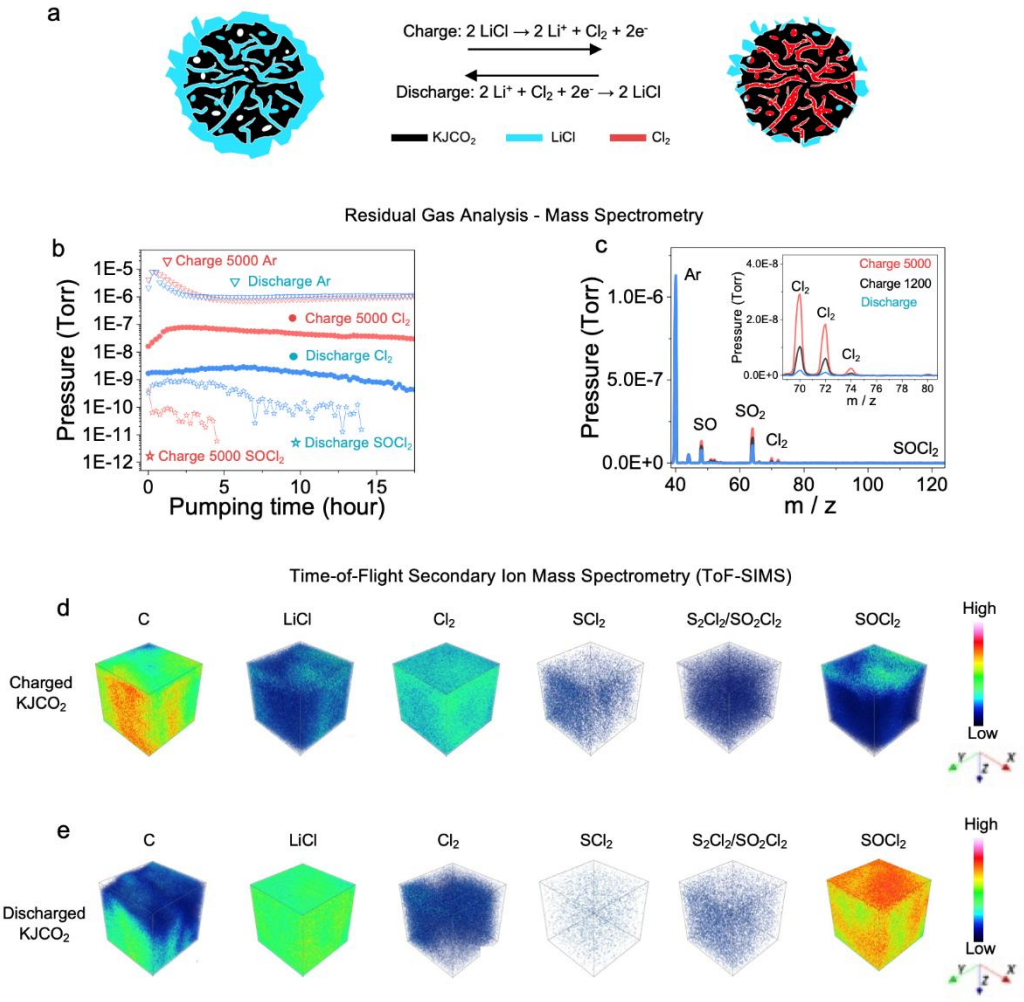

Figure 5. Battery reactions on the positive electrode side. a) Schematic drawing of the LiCl oxidation/Cl_2 reduction in $KJCO_2$ during charge and discharge, based on the reversible LiCl/Cl_2 redox reactions. b) The mass spectrometry detected pressure vs. vacuum pumping times of Ar, Cl_2, and $SOCl_2$ evolved from a $KJCO_2$ electrode charged to 5000 mAh g^{-1} and those evolved

from a discharged cell. Both cells were cycling at -40 °C when stopped for removing the positive electrodes for measurements. c) Mass spectrometry (after 17.5 hours vacuum pumping) of evolved species from $KJCO_2$ electrodes charged to 1200 or 5000 mAh g^{-1} and from discharged ones. Ar (*m/z* = 40 amu), Cl_2 (*m/z* = 70 amu), $SOCl_2$ (*m/z* = 118 amu). Inset shows Cl_2 with isotopes resolved. d, e) 3D distributions (Analysis area: 50 × 50 μm^2) of C, LiCl, Cl_2, SCl_2, S_2Cl_2/SO_2Cl_2 and $SOCl_2$ secondary ion fragments constructed from TOF-SIMS depth scan of a charged 5000 mAh g^{-1} $KJCO_2$ electrode (d) and fully discharged $KJCO_2$ electrode (e) evolved from -40 °C Li/$KJCO_2$ batteries.

SEM showed that not all of the surface LiCl coating was oxidizable to Cl_2 for subsequent reduction and battery cycling (Figure S8c), as observed previously.[20] When cycling/charging to higher capacities (i.e. 5000 mAh g^{-1}), LiCl in the carbon electrode was increasingly oxidized to Cl_2 accompanied by oxidation of $SOCl_2$ in electrolyte on carbon sites free of salt coating to form SCl_2/S_2Cl_2 and SO_2Cl_2 (see Figure 3e and Figure 4d, the increase in charging voltage).[20, 21] While most of the Cl_2 were trapped in the porous carbon for reversible reduction to LiCl in discharge (shown in battery retention experiments below),[20] we postulate that the more reactive SCl_2/S_2Cl_2 and SO_2Cl_2 species were poorly trapped, migrated into the electrolyte and shuttled to the Li anode side to cause chemical oxidation and corrosion. Such shuttling could lead to anode degradation, consumption of electrolyte that prevented 100% $SOCl_2$ regeneration and decreased battery cycling life.[20, 36]

We employed mass spectrometry to probe ex situ trapped species in $KJCO_2$ after cycling at - 40 °C by placing the electrodes under vacuum pumping for mass/charge (*m/z*) sampling of gaseous species evolved (see Methods, Figure S10 and Text S1). The detected Cl_2 escaping from a charged $KJCO_2$ electrode (to 5000 mAh g^{-1} or 1200 mAh g^{-1}) far exceed that from a discharged $KJCO_2$ (Figure 5b, c, Figure S11). The much lower Cl_2 detected in the latter was attributed to fragmentation of $SOCl_2$ in the residual electrolyte.[20,21]

Further, we performed 3D chemical mapping by time of flight - secondary ion mass spectroscopy (TOF-SIMS) depth profiling imaging of charged $KJCO_2$ (to 5000 mAh g^{-1} at -40 °C) and discharged $KJCO_2$ in 50 × 50 μm^2 by area regions (see Methods and Text S1). In charged $KJCO_2$, we detected low counts of LiCl and high counts of $Cl_2/SCl_2/S_2Cl_2/SO_2Cl_2$/carbon due to electro-oxidation of LiCl and $SOCl_2$, and more exposed carbon surfaces free of LiCl coating upon charging (Figure 5d). These species reduced while LiCl and $SOCl_2$ counts increased upon discharging (Figure 5e), confirming LiCl formation and regeneration of $SOCl_2$ (Text S1).

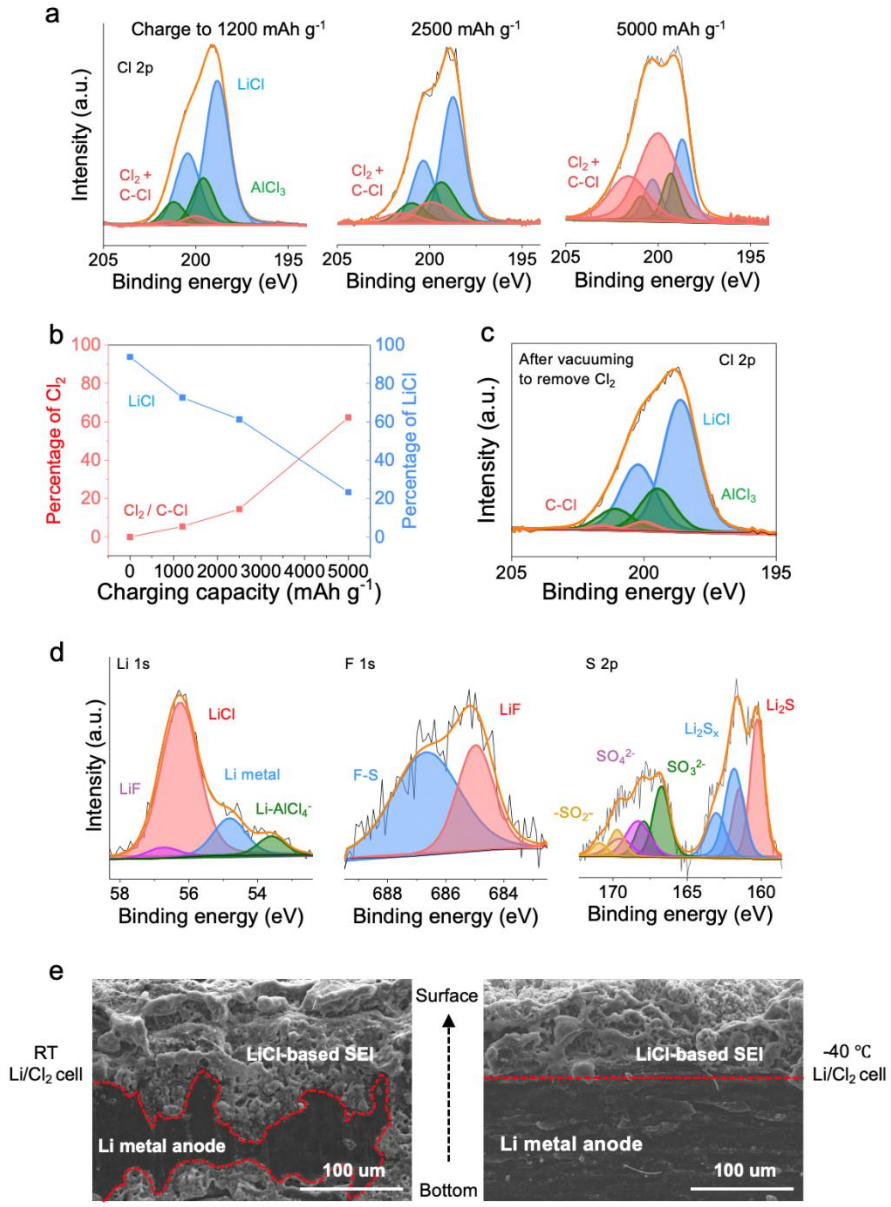

Figure 6. Battery reactions on the positive and negative electrode side. a) Cl 2p spectrum of $KJCO_2$ electrode after the -40 °C Li/$KJCO_2$ battery was charged to 1200, 2500, and 5000 mAh g^{-1}. Notice the red shaded components increase under increased charging, due to increased Cl_2 generated and trapped in $KJCO_2$. b) Percentages of Cl_2/C-Cl and LiCl species detected in charged $KJCO_2$ to different capacities analyzed from XPS fitting spectra (a). Increased charging led to clear decreases of LiCl and increases of Cl_2 detected. c) Cl 2p XPS spectrum of the charged 5000 mAh g^{-1} $KJCO_2$ electrode after pumping in vacuum for ~ 50 hours, showing much reduced Cl_2 species (in red shaded region under the curve), suggesting removal of trapped Cl_2 in $KJCO_2$. d) High-resolution XPS spectrum for Li 1s, F 1s and S 2p of the Li metal surface in a -40 °C Li/$KJCO_2$ battery after 10 cycles, respectively. e) Cross-sectional SEM images of Li metal anode in a Li/$KJCO_2$ battery after 10 cycles at room temperature (left) and -40 °C (right) with 100 mA g^{-1} current, respectively.

Lastly, we employed ex-situ XPS to probe species residing in $KJCO_2$ after charged to or discharged from 1200, 2500 and 5000 mAh g^{-1}, respectively (within hours of removal of electrodes from batteries, see Methods and Text S2) (reference binding energies for the compounds below can be found in Table S3). In all charged $KJCO_2$ we detected a peak in the Cl 2p spectrum at ~ 200 eV binding energy (**Figure 6**a, red lines) but not in discharged $KJCO_2$ (Figure S12). We attributed the ~ 200 eV peak to Cl_2 remaining trapped in the $KJCO_2$ and a small percentage of C-Cl, similar to our recent finding with Na/Cl_2 batteries.[37] The Cl_2 percentage increased with increasing charging capacity from 1200 to 5000 mAh g^{-1}, accompanied by decreases in the LiCl XPS signal on $KJCO_2$ (Figure 6a, b). Note that the same ~ 200 eV peak was reported for adsorbed molecular Cl_2 on Ag/AgCl at 100 K.[38]

The ~ 200 eV peak in the 5000 mAh g^{-1} charged $KJCO_2$ electrode significantly decreased (Figure 6c) after ~ 50 hours vacuum pumping (over which mass spectrometry detected little Cl_2 remaining in the electrode, Figure S13), indicating that Cl_2 remained in charged carbon electrode for up to ~ 2 days under vacuum. Afterwards a weak peak at ~ 200 eV peak remained (Figure S14a) and was attributed to C-Cl formed by chlorination of carbon during battery charging.[39] The C-Cl peak persisted after washing by deionized ultra-filtered (DIUF) water to remove all the residual LiCl, $AlCl_3$ (Figure S14b, c), but disappeared upon annealing at 600 °C in a N_2 atmosphere due to C-Cl bond breaking (Figure S14d). With charged $KJCO_2$ we also observed a peak at ~ 286.6 eV in the C 1s spectrum due to Cl bonding (Figure S15).[39] Note that, C-Cl could further interact with Cl_2 and possibly led to the formation of Cl_3^- upon batteries charging.[40] We performed Raman spectroscopy study of 1200 mAh g^{-1} charged amorphous carbon nanospheres[20] by sealing the electrode in an argon-filled aluminum pouch without exposed to air/water during the entire Raman measurement. However, we failed to observe the expected Raman peaks of Cl_3^- between 262 cm^{-1} and 280 cm^{-1} (Figure Figure S16).[41] The peaks present in the Raman spectrum were due to S_8, consistent with previous literature report.[42] Further investigation of possible Cl_3^- species in our system is needed.

Overall, the reactions of secondary Li/Cl_2 battery can be described as follows.[20, 21, 29] The first discharge was due to Li metal anode oxidation and $SOCl_2$ reduction into S, SO_2 and Cl^-. The Li^+ ions stripped from the Li anode react with Cl^-, resulting in the deposition of LiCl onto the carbon surface until passivation (Figure 2e-h).[20, 21, 29]

$$SOCl_2 + 4\ Li^+ + 4\ e^- \rightarrow S + SO_2 + 4\ LiCl \quad (1)$$

Upon charging, the deposited LiCl were increasingly oxidized/removed to Cl_2 (Figure S8a-c, Figure 5 and Figure 6a) accompanied by decreases in the battery electrochemical

impedance (Figure S9). The formation of Cl_2 constituted the main charging capacity according to the following reaction:[20, 21]

$$2\ LiCl \rightarrow 2\ Li^+ + Cl_2 + 2\ e^- \quad (2)$$

When cycling/charging to higher capacities (Figure 3e, Figure 4d), LiCl in the carbon electrode was increasingly oxidized to Cl_2 accompanied by oxidation of $SOCl_2$ in electrolyte on carbon sites free of salt coating. Possible oxidation reactions were proposed including:[20, 21]

$$SOCl_2 + AlCl_4^- \rightarrow AlCl_4^-\ SOCl^+ + \tfrac{1}{2}\ Cl_2 + e^- \quad (3)$$

$$SOCl_2 + SOCl^+AlCl_4^- + 2\ AlCl_4^- \rightarrow SCl^+AlCl_4^- + SO_2Cl_2 + Cl_2 + 2\ AlCl_3 + 2\ e^- \quad (4)$$

The $SCl^+AlCl_4^-$ was essentially a compound formed by $AlCl_3$ complexing with SCl_2. The SO_2 and S formed in the first discharge was soluble in the electrolyte. SO_2Cl_2 could form due to chemical reaction between SO_2 (formed after the first discharge) and Cl_2:[20, 21]

$$SO_2 + Cl_2 \rightarrow SO_2Cl_2 \quad (5)$$

Also, after enough Cl_2 was formed by charging, S could react with Cl_2 to form SCl_2, which could be further dissociated into S_2Cl_2 and Cl_2, according to the following reactions:[20, 21]

$$S + Cl_2 \rightarrow SCl_2 \quad (6)$$

$$2\ SCl_2 \leftrightarrow S_2Cl_2 + Cl_2 \quad (7)$$

These oxidation reactions led to Cl_2, SCl_2/S_2Cl_2, and SO_2Cl_2 (when Cl_2 was not trapped in the pores) during battery charging.[20, 21] During battery discharge (Figure 3e, Figure 4d), all the oxidation/charging products of the Li/Cl_2 battery were reversibly reduced, corresponding to:[20, 21]

$$2\ Li^+ + SCl_2 + 2\ e^- \rightarrow S + 2\ LiCl\ (\text{higher plateau}) \quad (8)$$

$$2\ Li^+ + S_2Cl_2 + 2\ e^- \rightarrow 2\ S + 2\ LiCl\ (\text{higher plateau}) \quad (9)$$

$$2\ Li^+ + Cl_2 + 2e^- \rightarrow 2\ LiCl\ (\text{main plateau}) \quad (10)$$

$$2\ Li^+ + SO_2Cl_2 + 2e^- \rightarrow SO_2 + 2\ LiCl\ (\text{lower plateau}) \quad (11)$$

We showed previously SO_2Cl_2 reduction occurred near the end of the main Cl_2 discharge plateau.[20, 21] The SCl_2/S_2Cl_2 were involved in the high discharge plateau (but with low capacity) before the main Cl_2 discharge, also reported previously.[20, 21] In addition, low temperature afforded higher reversible cycling capacity of the Li/Cl_2 batteries (near 100% CE), with the trapped oxidative species fully reduced to LiCl, and allowing ~ 100% regeneration of $SOCl_2$ through:[20, 21]

$$LiCl + AlCl_4^-\ SOCl^+ \rightarrow LiAlCl_4 + SOCl_2 \quad (12)$$

2.4. Trapping of reactive species in porous carbon and battery reversibility: temperature effects

Cycling of our Li/KJCO$_2$ batteries at higher specific capacities generated larger amounts of Cl_2, SCl_2/S_2Cl_2 and SO_2Cl_2 in the positive electrode side during charging. These species were highly reactive and could shuttle to Li anode to damage the SEI and corrode the underlying Li metal. When such side reaction was severe, higher than 100% CE was observed suggesting that the Li/SEI layer equilibrium was broken by the shuttled species, and the Li metal became more exposed and could discharge beyond the deposited Li by charging (i.e., at room temperature and -20 ℃, Figure S5a-d). For batteries stably cycling with ~ 100 % average CE over > 100 cycles, such as Li/KJCO$_2$ cells cycling at 1200 mAh g^{-1} at -40 ℃ (Figure 3a), reactive species were effectively trapped in the carbon positive electrodes with little shuttling effect. This was corroborated with battery retention result that when we held a battery charged to 1200 mAh g^{-1} at - 40 ℃ at open-circuit for 3 days and then discharged the battery, the battery retained ~ 100% CE without any capacity loss (Figure S17a). The retention experiment was repeated several times during cycling over > 100 cycles (Figure S17a).

When a Li/KJCO$_2$ battery was charged at -40 ℃ and warmed to room temperature to hold for 3 days at open circuit, we observed that the main discharge plateau at ~ 3.3 V decreased in capacity while the lower discharge plateau at ~ 3.10 V extended, accompanied by reduced battery cycle life to < 30 cycles (Figure S17b). The ~ 3.10 V plateau was attributed to the reduction of SO_2Cl_2 formed by reactions between SO_2 and escaped Cl_2, due to reduced Cl_2 trapping by KJCO$_2$ at higher temperature.[20] A high CE of > 120 % following the retention again indicated shuttling effect. Shuttling effect became more evident and led to shorter cycle-life of a Li/KJCO$_2$ battery with a lower amount of electrolyte (75 μL, Figure S18).

Temperature dependent battery characteristics suggested that trapping of reactive species in the porous carbon was more effective at lower temperature, preventing shuttling, allowing higher reversible cycling capacity and ~ 100% regeneration of $SOCl_2$ (consumed in the charging step) via $LiCl + AlCl_4^- SOCl^+ \rightarrow LiAlCl_4 + SOCl_2$.[20] Complete trapping/retention of electro-oxidation generated species in the positive electrode is therefore critical to prolong the cycle life of our batteries.

Unique to the battery characteristics cycling at -80 ℃ was that increasing charging capacity from 1200 mAh g^{-1} to ~ 5000 mAh g^{-1} led to more extended high discharge voltage plateaus at ~ 3.8 V (well above the Cl_2 reduction voltage plateau of ~ 3.1 V, Figure 4d), and no obvious capacity loss of the 3.8 V voltage plateau was observed after one-day-retention experiment at -80 ℃ (Figure S19), suggesting efficient trapping and reduction of SCl_2/S_2Cl_2

generated in the charging step at -80 °C, The 3.8 V discharge plateau was nearly non-existent in batteries operated at -40 °C (1200 to 5000 mAh g^{-1}, Figure 3e), suggesting escaping of these species from the positive electrodes without subsequent electro-reduction during discharging.

Taken together, at room temperature Li/Cl_2 batteries exhibited reversible Li/Li^+ and Cl^-/Cl_2 redox at capacity of ~ 1200 mAh g^{-1} (discharge voltage ~ 3.5 V) with $KJCO_2$ in the positive electrode effectively trapping Cl_2 in its abundant nanoscale pores. At a lower temperature of -40 °C, the reversible capacity limit for Cl^-/Cl_2 redox (discharge voltage ~ 3.3 V) increased to ~ 2500 mAh g^{-1}, owing to increased trapping of Cl_2 in $KJCO_2$ at -40 °C. At an even lower -80 °C, the reversible capacity limit for Cl^-/Cl_2 redox further increased to ~ 4000 mAh g^{-1}, and the even more reactive species such as SCl_2/S_2Cl_2 were retained on the positive electrode side, giving a high discharge plateau at ~ 3.8 V with up to 1000 mAh g^{-1} capacity. These batteries all showed longer cycle lives at lower temperatures under lower cycling capacities due to reduced shuttling effects. Hence, developing new materials with higher porosity and strong molecular trapping ability for positive electrodes of Li/Cl_2 batteries will be a key to boost the capacity of this type of new battery with prolonged cycling life.

2.5. Solid-electrolyte interface at the Li negative electrode

Lastly, we investigated the SEI chemistry on the Li metal negative electrode side by ex-situ XPS characterization after removed from a Li/$KJCO_2$ battery cycling at -40 °C for 10 cycles (total cycle life > 130) at 1200 mAh g^{-1} (reference binding energies for the compounds below can be found in Table S4). The dominant composition in the SEI on the Li electrode was LiCl formed immediately upon exposure of Li to the electrolyte due to reaction with $SOCl_2$ (Figure 6d). Existence of LiF in the SEI was identified (Figure 6d), attributed to reactions between Li with FSI- additive in our electrolyte.[20, 43-46] Similar to Na/Cl_2 battery and other alkali metal batteries in general,[20, 43-46] the fluoride component imparted higher stability to the SEI and cycling stability of the battery (Figure S20). In addition to LiCl and LiF, the SEI also contained F-S related species (FSI^- decomposition, Figure 6d), -SO_2-, Li_2SO_4, Li_2SO_3, Li_2S, Li_2S_x, (Figure 6d), $AlCl_3$ (Figure S21), and SiO_2 (residue from separator, Figure S21),[20, 47-49] suggesting reactions between the Li metal and species in the electrolyte including the reactive species from the positive electrode (Cl_2, SCl_2, SO_2Cl_2) shuttled to the Li side.[20]

We perform SEM imaging of the cross-sectional Li electrodes and observed SEI layers on top of the Li metal. The SEI layer on Li in a battery after cycling at room temperature was thicker and much more irregular than that formed with -40 °C (Figure 6e). This was attributed to stronger shuttling effect and more severe side reactions/corrosions of Li due to reactive

species escaped from the positive electrode, consistent with the reduced cycling performance of Li/Cl_2 batteries (Figure S5a, b) and poorer retention of reactive species at higher temperature (Figure S17b). The -40 °C Li/Li symmetric cell also showed reversible Li deposition/stripping over 3500 h cycling (~146 cycles, 24 hours per cycle, Figure S22), which was more stable than cycling of the Li/$KJCO_2$ battery at the same current density (~130 cycles, Figure 3a). Shuttling effect in the Li/$KJCO_2$ full cell could led to faster decay of the Li metal anode more than in Li/Li cell.

Note that $SOCl_2$ is toxic and could release hydrochloric acid upon contact with water and alcohols. However, well-sealed primary Li/$SOCl_2$ batteries have been highly safe and are widely available commercially for industrial and household use from sources such as Amazon. Our rechargeable low temperature cells are well contained in coin cells and have also been highly safe in our lab thus far without any incidents out of hundreds of cells made and tested, consistent with strong trapping of volatile species generated. Besides, the Ni current collector surface was found to be passivated by $NiCl_2$/NiO layer during cycling, avoiding further corrosion of the underlying Ni metal (Figure S23). We explored other current collectors and found Li/$KJCO_2$ batteries with $KJCO_2$ loaded on 316 stainless-steel (SS) mesh or just 316 SS coin cell case (without current collector) were cyclable at 1200 mAh g^{-1} at -40 °C (see Methods, Figure S24).

We also succeeded in assembling and operating Li/Cl_2 pouch-type cells towards scaling such batteries to large sizes and stacks. In terms of high energy density, the next steps are to increase the carbon electrode mass loading and reduce electrolyte volume/mass. To give a perspective, we estimate that an energy density of ~ 370 Wh kg^{-1} can be reached when cycled at 2500 mAh g^{-1} specific capacity using a $KJCO_2$ loading of 4 mg cm^{-2} and a lower electrolyte amount of 50 µL in the CR2032 coin cell (as shown in our previous work).[20] The estimate included mass of the electrolyte, Li metal, carbon, and separators. We are currently optimizing the energy density of our Li/$KJCO_2$ battery.

3. Conclusions

We developed a novel activated carbon for rechargeable Li batteries in a newly designed $SOCl_2$ based electrolyte exhibiting low viscosity and high conductivity down to low temperatures. The resulting battery delivered reversible capacity in the range of 1200 - 5000 mAh g^{-1} with useful cycle lives at down to -40 °C and -80 °C. Investigations by XPS and mass spectrometry revealed Cl_2 and SCl_2/S_2Cl_2 generated by oxidation of LiCl and $SOCl_2$ during battery charging and trapped in the pore of activated carbon. Low temperatures enhanced

trapping of highly oxidative species, slowed down shuttling effects and impeded rapid thickening of the passivating SEI layer on the Li metal anode. The Li/$KJCO_2$ cells are different from other types of secondary batteries in that lower temperatures afford higher battery capacities/energy densities and longer cycle lives than at RT. Battery reversibility relies on trapping of redox active species in the positive electrode and involves electrolyte reaction and regeneration. Innovations in porous carbon and non-carbon (i.e., metal-organic framework MOF[50]) materials for positive electrodes could further improve such batteries towards wide-spread applications.

Supporting Information

Supporting Information is available from the Wiley Online Library or from the author.

Acknowledgements

Peng Liang and Guanzhou Zhu contributed equally to this work. This work was supported by Deng Family gift. Part of this work was performed at the Stanford Nano Shared Facilities (SNSF), supported by the National Science Foundation under award ECCS-2026822.

Contributions

P.L., G.Z., and H.D conceived the project, performed the characterizations, analysed the data and wrote the paper. C.-L.H. and Y.-Y.L. performed the KJ activation experiments and SEM measurements. H.S. and B.Y. performed the TOF-SIMS experiments. P.L., G.Z., H.D, S.-C.W, J.L., F.W., and B.-J.H interpreted the data.

Conflict of Interest

The authors declare no conflict of interest.

Data Availability Statement

The data that support the findings of this study are available from the corresponding author upon reasonable request.

References

[1] X. Fan, X. Ji, L. Chen, J. Chen, T. Deng, F. Han, J. Yue, N. Piao, R. Wang, X. Zhou, X. Xiao, L. Chen, C. Wang. *Nat. Energy* **2019**, *4*, 882.

[2] M. C. Smart, B. V. Ratnakumar, R. C. Ewell, S. Surampudi, F. J. Puglia, R. Gitzendanner. *Electrochim. Acta* **2018**, *268*, 27.

[3] A. Gupta, A. Manthiram. *Adv. Energy Mater*. **2020**, *10*, 2001972.

[4] C. K. Huang, J. S. Sakamoto, J. Wolfenstine, S. Surampudi. *J. Electrochem. Soc*. **2000**, *147*, 2893.

[5] E. J. Plichta, M. Hendrickson, R. Thompson, G. Au, W. K. Behl, M. C. Smart, B. V. Ratnakumar, S. Surampudi. *J. Power Sources* **2001**, *94*, 160.

[6] Q. Li, S. Jiao, L. Luo, Orcid, M. S. Ding, J. Zheng, S. S. Cartmell, C.-M. Wang, K. Xu, J.-G. Zhang, W. Xu. *ACS Appl. Mater. Interfaces*. **2017**, *9*, 18826.

[7] N. Zhang, T. Deng, S. Zhang, C. Wang, L. Chen, C. Wang, X. Fan. *Adv. Mater*. **2022**, *34*, 2107899.

[8] A. Fly, I. Kirkpatrick, R. Chen. *Appl. Therm. Eng*. **2021**, *189*, 116750.

[9] G. Nagasubramanian. *J. Appl. Electrochem*. **2001**, *31*, 99.

[10] S. S. Zhang, K. Xu, T. R. Jow. *Electrochim. Acta* **2004**, *49*, 1057-1061.

[11] J.-Y. Liang, Y. Zhang, S. Xin, S.-J. Tan, X.-H. Meng, W.-P. Wang, J.-L. Shi, Z.-B. Wang, F. Wang, L.-J. Wan, Y.-G. Guo. *Angew. Chem. Int. Ed*. **2023**, *135*, e20230038.

[12] D. Hubble, D. E. Brown, Y. Zhao, C. Fang, J. Lau, B. D. McCloskey, G. Liu. *Energy Environ. Sci*. **2022**, *15*, 550.

[13] B. Liao, H. Li, M. Xu, L. Xing, Y. Liao, X. Ren, W. Fan, L. Yu, K. Xu, W. Li. *Adv. Energy Mater*. **2018**. *8*, 1800802.

[14] E. J. Plichta, W. K. Behl. *J. Power Sources* **2000**, *88*, 192.

[15] J. Holoubek, H. Liu, Z. Wu, Y. Yin, X. Xing, G. Cai, S. Yu, H. Zhou, T. A. Pascal, Z. Chen, P. Liu. *Nat. Energy* **2021**, *6*, 303.

[16] J. Qin, Q. Lan, N. Liu, Y. Zhao, Z. Song, H. Zhan. *Energy Storage Mater*. **2020**, *26*, 585-592 (2020).

[17] Z. Zhu, W. Wang, Y. Yin, Y. Meng, Z. Liu, T. Jiang, Q. Peng, J. Sun, W. Chen. *J. Am. Chem. Soc*. **2021**, *143*, 20302.

[18] J. Li, L. Wang, Y. Zhao, S. Li, X. Fu, B. Wang, H. Peng. *Adv. Funct. Mater*. **2020**, *30*, 2001619.

[19] M. Qiu, P. Sun, K. Han, Z. Pang, J. Du, J. Li, J. Chen, Z. L. Wang, W. Mai. *Nat. Commun*. **2023**, *14*, 601.

[20] G. Zhu, X. Tian, H.-C. Tai, Y.-Y. Li, J. Li, H. Sun, P. Liang, M. Angell, C.-L. Huang, C.-S. Ku, W.-H. Hung, S.-K. Jiang, Y. Meng, H. Chen, M.-C. Lin, B.-J. Hwang, H. Dai, *Nature.* **2021**, *596*, 525.

[21] G. Zhu, P. Liang, C.-L. Huang, C.-C. Huang, Y.-Y. Li, S.-C. Wu, J. Li, F. Wang, X. Tian, W.-H. Huang, S.-K. Jiang, W.-H. Hung, H. Chen, M.-C. Lin, B.-J. Hwang, H. Dai. *J. Am. Chem. Soc*. **2022**, *144*, 22505.

[22] H. V. Venkatasetty, D. J. Saathoff. *J. Electrochem. Soc*. **1981**, *128*, 773.

[23] K. A. Klinedinst, M. J. Domeniconi. *J. Electrochem. Soc*. **1980**, *127*, 539.

[24] K. M. Abraham, L. Pitts, W. P. Kilroy. *J. Electrochem. Soc*. **1985**, *132*, 2301.

[25] C. R. Schlaikjer, F. Goebel, N. Marincic. *J. Electrochem. Soc*. **1979**, *126*, 513.

[26] B. Chen, R. Li, G. Ma, X. Gou, Y. Zhu, Y. Xia. *Nanoscale* **2015**, *7*, 20674.

[27] C. Y. Tsai, H. C. Tai, C. A. Su, L. M. Chiang, Y. Y. Li. *ACS Appl. Nano Mater*. **2020**, *3*, 10380.

[28] H. G. Jung, J. Hassoun, J. B. Park, Y. K. Sun, B. Scrosati. *Nat. Chem*. **2012**, *4*, 579.

[29] K. M. Abraham, R. M. Mank. *J. Electrochem. Soc*. **1980**, *127*, 2091.

[30] B. J. Carter, R. M. Williams, F. D. Tsay, A. Rodriguez, S. Kim, M. M. Evans, H. Frank. *J. Electrochem. Soc*. **1985**, *132*, 525.

[31] D. Wang, J. Jiang, Z. Pan, Q. Li, J. Zhu, L. Tian, P. K. Shen. *Front. Mater. Sci*. **2019**, *6*, 245.

[32] N. Marinčić. *J. Appl. Electrochem.* **1976**, *6*, 51.

[33] T. I. Evans, T. V. Nguyen, R. E. White. *J. Electrochem. Soc*. **1989**, *136*, 328.

[34] S. Gilman, W. Wade. *J. Electrochem. Soc*. **1980**, *127*, 1427.

[35] K. Yan, J. Wang, S. Zhao, D. Zhou, B. Sun, Y. Cui, G. Wang. *Angew. Chem. Int. Ed*. **2019**, *131*, 11486.

[36] K. M. Abraham. *J. Power Sources* **1991**, *34*, 81.

[37] G. Zhu, P. Liang, C.-L. Huang, S.-C. Wu, C.-C. Huang, Y.-Y. Li, S.-K. Jiang, W.-H. Hung, J. Li, F. Wang, B.-J. Hwang, H. Dai. *Proc. Natl. Acad. Sci. U.S.A*. **2023**, DOI: 10.1073/pnas.2310903120.

[38] H. Piao, K. Adib, M. A. Barteau. *Surf. Sci*. **2004**, *557*, 13.

[39] X. Zhang, T. Schiros, D Nordlund., Y. C. Shin, J. Kong, M. Dresselhaus, T. Palacios. *Adv. Funct. Mater*. **2015**, *25*, 4163.

[40] J. C. Evans, G. Y.-S. Lo. *J. Chem. Phys*. **1966**, *44*, 3638.

[41] R. Brückner, H. Haller, M. Ellwanger, S. Riedel. *Chem. Eur. J*. **2012**, *18*, 5741.

[42] C. Nims, B. Cron, M. Wetherington, J. Macalady, J. Cosmidis. *Sci. Rep*. **2019**, *9*, 7971.

[43] J, Auvergniot, A. Cassel, D. Foix, V. Viallet, V. Seznec, R. D. Redox. *Solid State Ion*. **2017**, *300*, 78.

[44] P. Liang, H. Sun, C.-L. Huang, G. Zhu, H.-C. Tai, J. Li, F. Wang, Y. Wang, C.-J. Huang, S.-K. Jiang, M.-C. Lin, Y.-Y. Li, B.-J. Hwang, C.-A. Wang, H. Dai *Adv Mater.* **2022**, *34*, 2207361.

[45] H. Sun, G. Zhu, Y. Zhu, M.-C. Lin, H. Chen, Y.-Y. Li, W. H. Hung, B. Zhou, X. Wang, Y. Bai, M. Gu, C.-L. Huang, H.-C. Tai, X. Xu, M. Angell, J.-J. Shyue, H. Dai, *Adv. Mater*. **2020**, *32*, 2001741.

[46] H. Sun, P. Liang, G. Zhu, W. H. Hung, Y.-Y. Li, H.-C. Tai, C.-L. Huang, J. Li, Y. Meng, M. Angell, C.-A. Wang, H. Dai, *Proc. Natl. Acad. Sci. U.S.A*. **2020**, *117*, 27847.

[47] X.-Q. Zhang, X. Chen, L.-P. Hou, B.-Q. Li, X.-B. Cheng, J.-Q. Huang, Q. Zhang. *ACS Energy Lett*. **2019**, *4*, 411.

[48] Y. Fu, C. Zu, A. Manthiram. *J. Am. Chem. Soc*. **2013**, *135*, 18044.

[49] G. M. Ingo, C. Riccucci, G. Bultrini, S. Dirè, G. Chiozzini. *J. Therm. Anal. Calorim*. **2001**, *66*, 37.

[50] Y. Xu, L. Jiao, J. Ma, P. Zhang, Y. Tang, L. Liu, Y. Liu, H. Ding, J. Sun, M. Wang, Z. Li, H.-L. Jiang, W. Chen, *Joule*. **2023**, *7*, 515.